# Supplementary Information
# Direct laser writing breaking diffraction barrier based on two-focus parallel peripheral-photoinhibition lithography

**Dazhao Zhu,[a†] Liang Xu,[b†] Chenliang Ding,[a] Zhenyao Yang,[a] Yiwei Qiu,[a] Chun Cao,[a] Hongyang He,[c] Jiawei Chen,[c] Mengbo Tang,[a] Lanxin Zhan,[a] Xiaoyi Zhang,[a] Qiuyuan Sun,[a] Chengpeng Ma,[a] Zhen Wei,[a] Wenjie Liu,[a,b] Xiang Fu,[d] Cuifang Kuang,[a,b,*] Haifeng Li,[a,b] Xu Liu [a,b,*]**

[a]Research Center for Intelligent Chips and Devices, Zhejiang Lab, Hangzhou 311100, China
[b]State Key Laboratory of Modern Optical Instrumentation, College of Optical Science and Engineering, Zhejiang University, Hangzhou 310027, China
[c]State Key Laboratory of Industrial Control Technology, College of Control Science and Engineering, Zhejiang University, Hangzhou 310027, China
[d]Research Center for Humanoid Sensing, Zhejiang Lab, Hangzhou 311100, China

*****Cuifang Kuang**,** E-mail: cfkuang@zju.edu.cn
*****Xu Liu**,** E-mail: liuxu@zju.edu.cn
†These authors contributed equally to this work.

## 1 System Configuration

Figure S1 shows the physical arrangement of the proposed parallel peripheral-photoinhibition lithography ($P^3L$) system. The excitation beam wavelength is 780 nm (Coherent, Chameleon Vision II, 3 W, Glasgow, UK; pulsed 80-MHz repetition rate), and that of the inhibition beam is 532 nm (Laser Quantum, Opus 532-5W, Stockport, UK, continuous wave). The 780-nm pulsed laser successively passes through the isolator (EOT, 110-22051-0001, Traverse City, USA), a half-wave plate (1/2 WP, LBTEK, HWP10-780B, Changsha China), and a polarizing beam splitter (PBS, Union Optic, PBS9025-620-1000, Wuhan China); then, it is reflected into Module 1. Because the laser output power cannot be adjusted directly, the beam power passing through the PBS is controlled by rotating the 1/2 WP. The other beam reflected by the PBS is blocked for safety. The 532-nm continuous laser enters Module 2 directly.

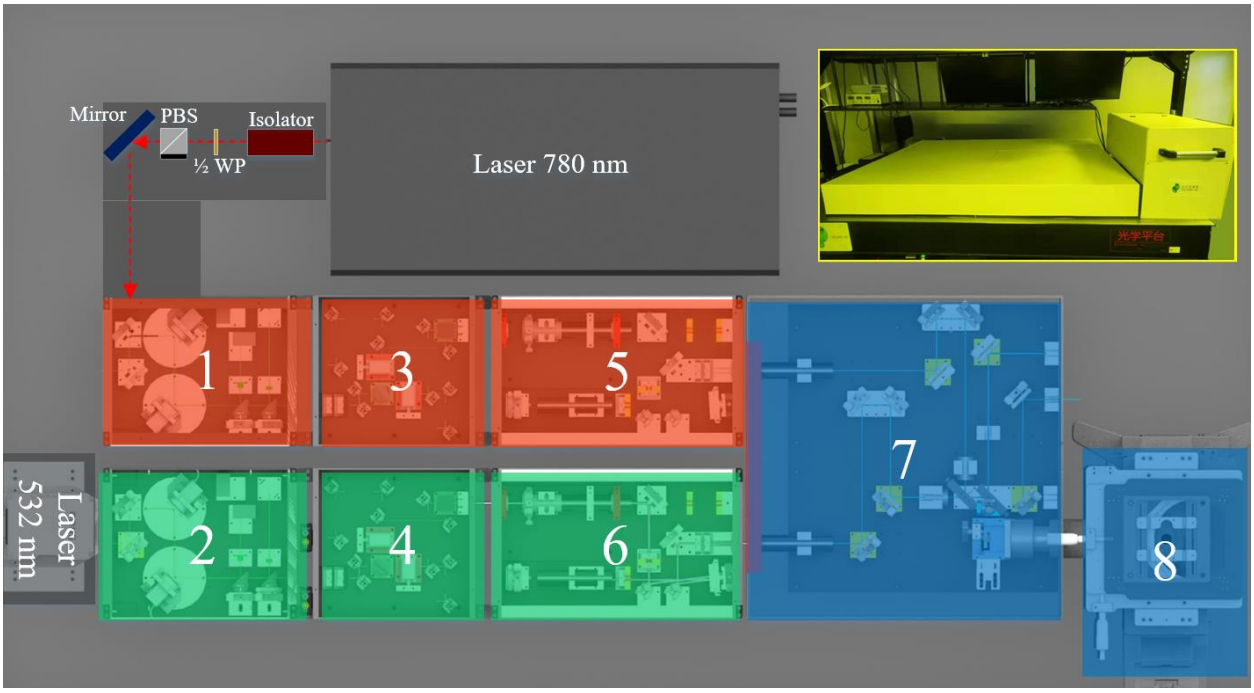


**Fig. S1** Physical arrangement of the proposed eight-module system. A photograph of the instrument is included in the inset. PBS: polarizing beam splitter; ½ WP: half-wave plate.

Figure S2 provides a schematic of Module 2. Plate glasses s5 and s6 reflect 2% of the beam energy, which is focused by lenses s7 and s8 onto position sensors s10 and s11. Mirrors s3 and s4 adjust the beam path by the holder with the actuator whenever a position fluctuation is detected by s10 and s11. Module 1 is similar to Module 2; the only differences are the beam entrance position and the orientation of mirror s2, as illustrated by the dashed boxes in Fig. S2.

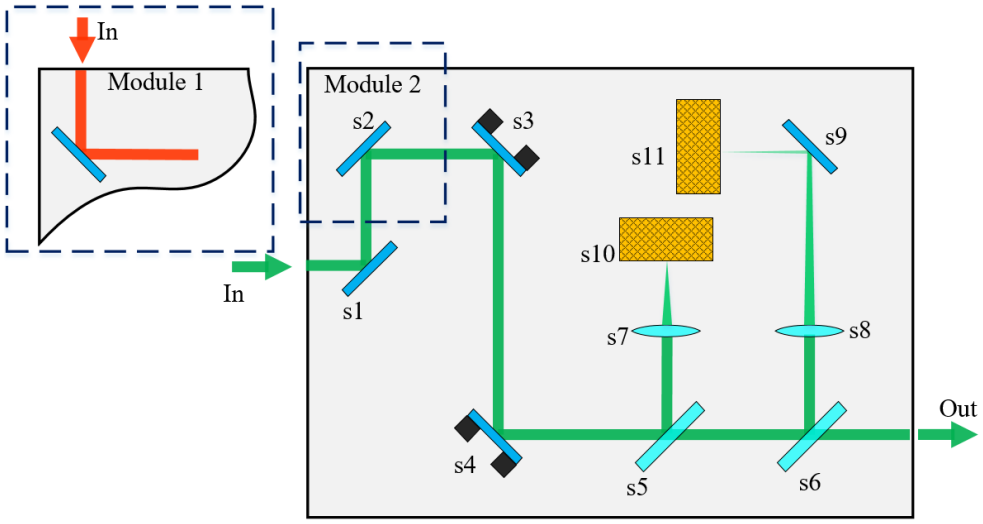


**Fig. S2** Schematic of Module 2: mirrors s1, s2, s3, s4, and s9; plate glasses s5 and s6; lenses s7 and s8; and position sensors s10 and s11. Module 1 is similar to Module 2, except for the entrance position and orientation of s2 (see the dashed boxes).

Modules 3 and 4 are used for on-off switching and the power adjustment of each beam. As shown in Fig. S3, 1/2 WP p1 is used to adjust the power ratio between the two polarized components. The beam is split into orthogonally polarized sub-beams i and ii (sub-beams iii and iv in Module 3) using PBS p4. The on-off switching and power are controlled by two acoustic–optical modulators (Module 3: AA Opto Electronic, MT110-A1.5-IR, p5 and p6 in Fig. S3; Module 4: AA Opto Electronic, MT110-A1.5-VIS, Orsay, France). Then, the two sub-beams are combined by another PBS (p11) placed immediately before the exit of the module.

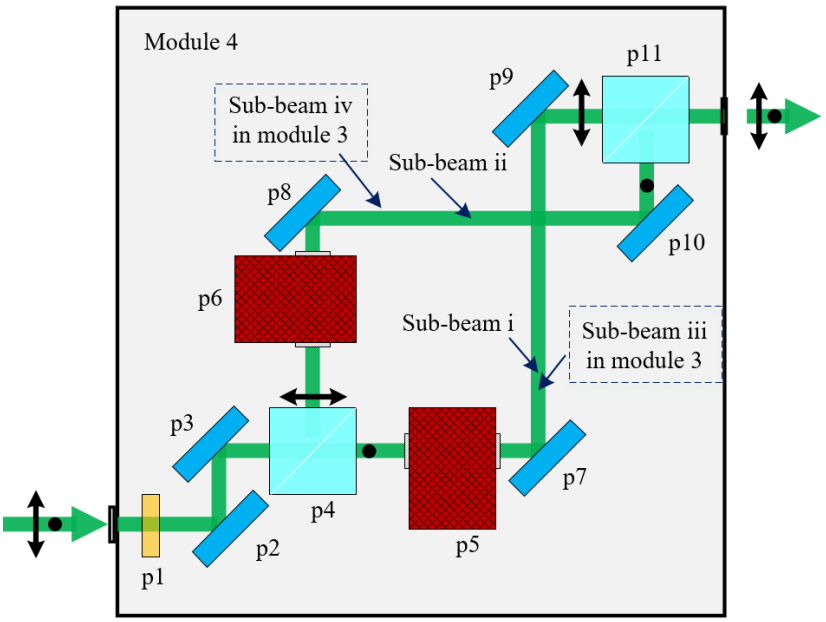


**Fig. S3** Schematic of Module 4 (Module 3 is the same except as indicated): ½ WP p1; mirrors p2, p3, p7, p8, p9, and p10; PBSs p4 and p11; and acoustic–optical modulators p5 and p6.

Modules 5 and 6 are mainly used for phase modulation by a spatial light modulator (SLM) (Module 5: Hamamatsu, X15223-02; Module 6: Hamamatsu, X15223-16, Hamamatsu, Japan), as shown in Fig. S4 (a). The diameter of the beam entering the module is firstly enlarged by a telescope consisting of lenses m1 and m3, and pinhole m2 is placed as a filter in the focal plane to maintain the Gaussian shape of the beam. The beam contains two components (sub-beams i and ii), which are reflected and modulated twice by the SLM. First, sub-beam i is modulated and reflected by the half-screen of the SLM. However, owing to the polarization properties of the SLM, sub-beam ii is not affected. The polarization directions of sub-beams i and ii are then exchanged by passing them twice through quarter-wave plate m7. Therefore, sub-beam ii can be modulated by the other half-screen of the SLM, with sub-beam i remaining unaffected (Fig. S4(b)). Finally, the beam is circularly polarized by another quarter-wave plate, m12.

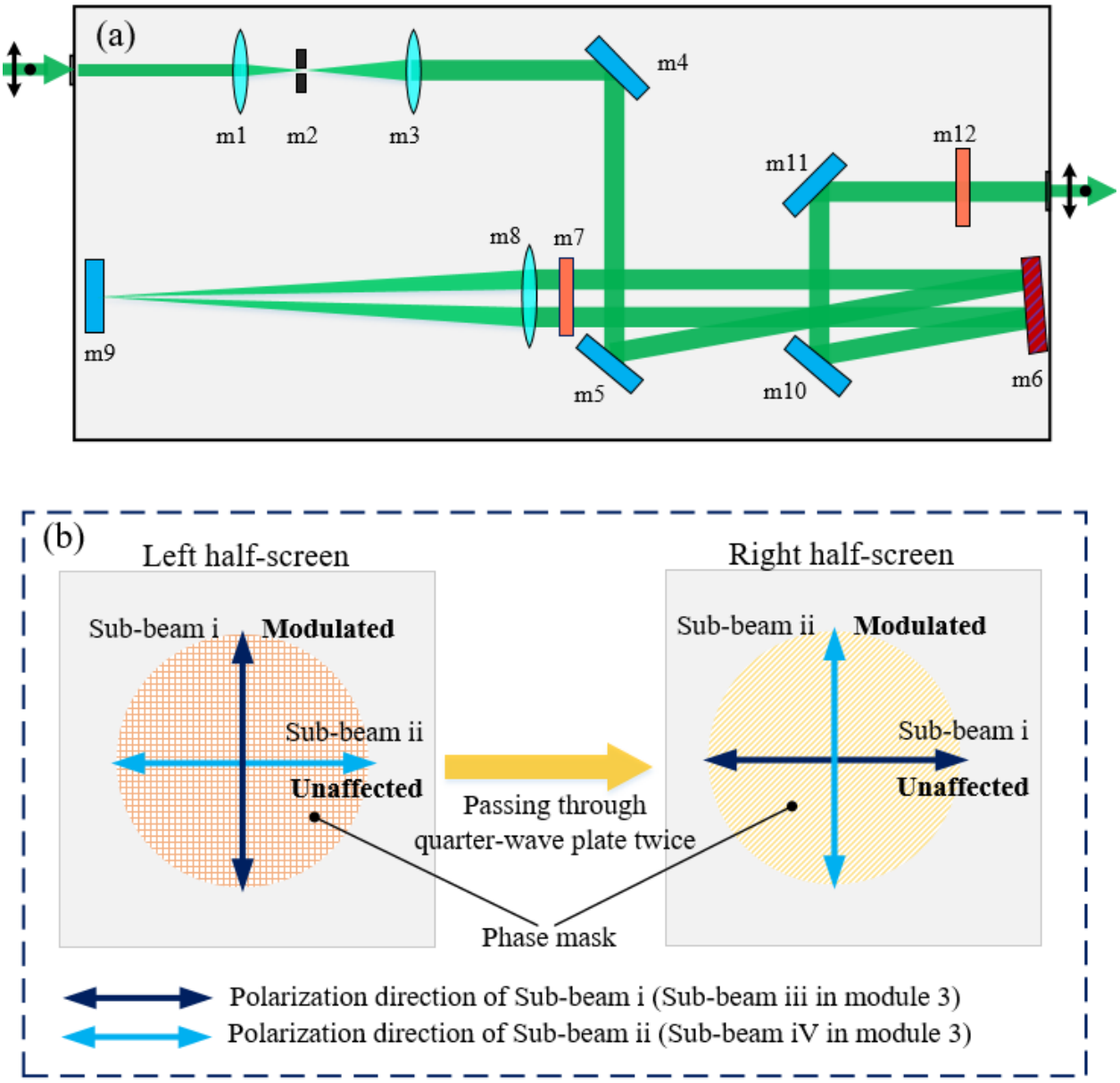


**Fig. S4** Schematic of Modules 5 and 6. (a) System configuration: mirrors m4, m5, m9, m10, and m11; lenses m1, m3, and m8; SLM m6; and quarter-wave plates m7 and m12. (b) Theory of identical modulation of sub-beams by the SLM.

The 532- and 780-nm beams (each including two sub-beams) are combined in Module 7, as shown in Fig. S5, using dichroic mirror c7. Lenses c1 and c6, as well as c8 and c12, are utilized to reduce the diameter of the corresponding beam to fit the pupil. Further, the screen of the SLM is imaged to charge-coupled device (CCD) camera c16 (HIK VISION, MV-CE200-10UM,

Hangzhou, China), which acts as a monitor. Mirrors c2, c3, c5, c9, c10, and c11 are used to ensure that the 532- and 780-nm beams pass through the same optical length. The combined beam is reflected into the galvanometer scanner (Cambridge Technology Inc, CTI-8310K, Lexington, USA) by split mirror c13, and 10% of the energy passes through c13 and enters CCD camera c16. The reflected light is detected using photomultiplier tube c19 (Hamamatsu, H10682-1, Hamamatsu, Japan), and imaging nanobeads are used to verify the spot quality. After passing through scan lens c15 (Nikon, PROJ-XSDD007835 A1, Tokyo, Japan), the combined beam exits the module.

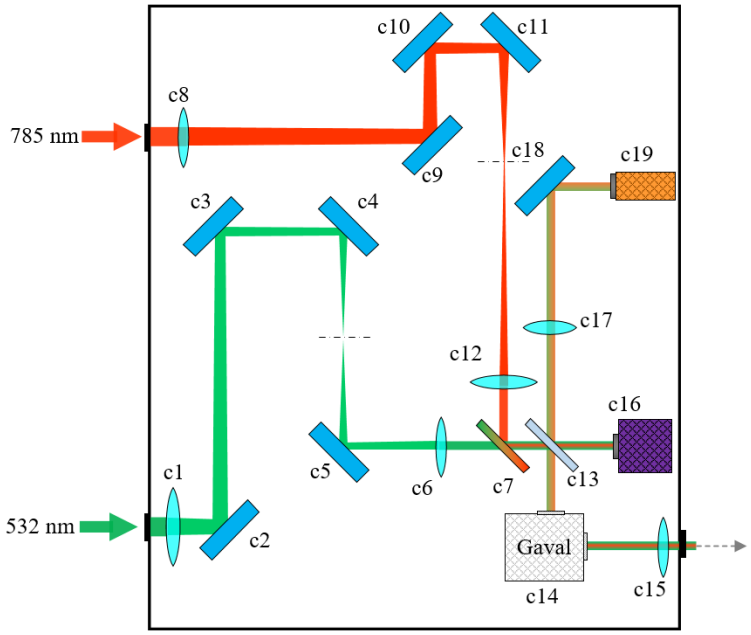


**Fig. S5** Schematic of Module 7: mirrors c2, c3, c4, c5, c9, c10, c11, and c18; lenses c1, c6, c8, c12, and c17; dichroic mirror c7; split mirror c13; galvanometer scanner c14; scan lens c15; CCD camera c16; and photomultiplier-tube detector c19.

Module 8 consists of a commercial microscope (Nikon, Ti-2e, Tokyo, Japan) with objective lenses (Nikon, NA 1.45, 100×, Tokyo, Japan. Olympus, NA 1.4, 40 ×, Tokyo, Japan). A high-precision X-Y stage with a movement range of 120 × 72 mm (Prior, HLD117DM, Cambridge, UK)

is used to extend the fabrication range. Further, an x-y-z stage with a movement range of 300 μm × 300 μm × 300 μm (PI, P-563.3CD, Karlsruhe, Germany) is employed for high-precision focusing.

## 2 Printing Two Lines of Text

To present the features of our system concisely, two solid spots superposed by the respective doughnut spots were used to print two lines of text (Figure S6(a) and (b)), with each spot printing one line. The distance between the two spots was 5.4 μm, and the speed was 10 mm/s. The powers of the single solid and inhibition spots were 12.6 and 40.0 mW, respectively. Figure S6(d) shows a scanning electron microscopy (SEM; Zeiss Sigma300, Germany) image. The printing process was recorded by a CCD camera (HIKROBOT, MV-CE200-10GM, Hangzhou, China) in the wide-field microscopy regime. To observe the pattern clearly using the CCD camera, the pattern was printed 10 times at the same lateral position but at different heights (Figure S6(c)). The z-direction movement was realized by a piezo stage (PI, P-563.3CD, Karlsruhe, Germany); the step size was 100 nm in the x, y, and z directions.

Figures S7(a) and S7(b) show the phase masks used to modulate the inhibition and excitation beams, respectively. To avoid the influence of zero-order light, a Fresnel lens phase was added. A grating phase was used to eliminate stray light. Moreover, all the aforementioned phases were superimposed with a corresponding flat map (provided by the SLM manufacturer). Figure S7(c) shows the four instants in the 5-s printing process for the two lines, and the complete procedure can be found in the supplementary video file.

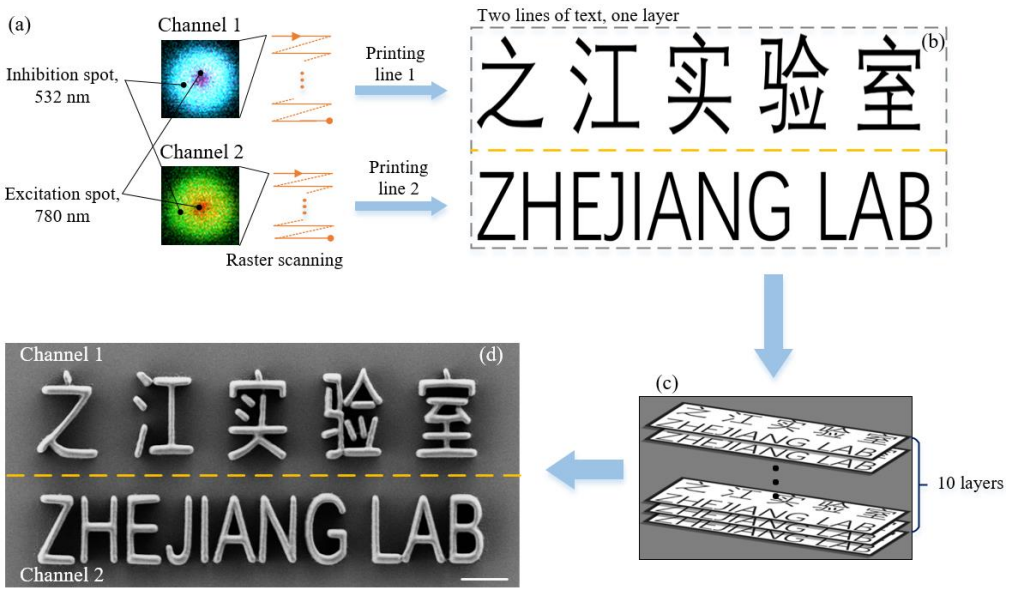


**Fig. S6** Printing of two lines of text by the proposed P$^3$L. (a) Two channels: channel 1 includes sub-beam i (532 nm) and sub-beam iii (780 nm); channel 2 includes sub-beam ii (532 nm) and sub-beam iv (780 nm). (b) Pattern of the two lines of text to be printed. The two channels perform raster scanning; channel 1 prints line 1, and channel 2 prints line 2, as shown in (b). (c) Ten layers were printed. (d) SEM image of two parallel lines of text printed by the proposed P$^3$L system. Scale bar: 2 μm.

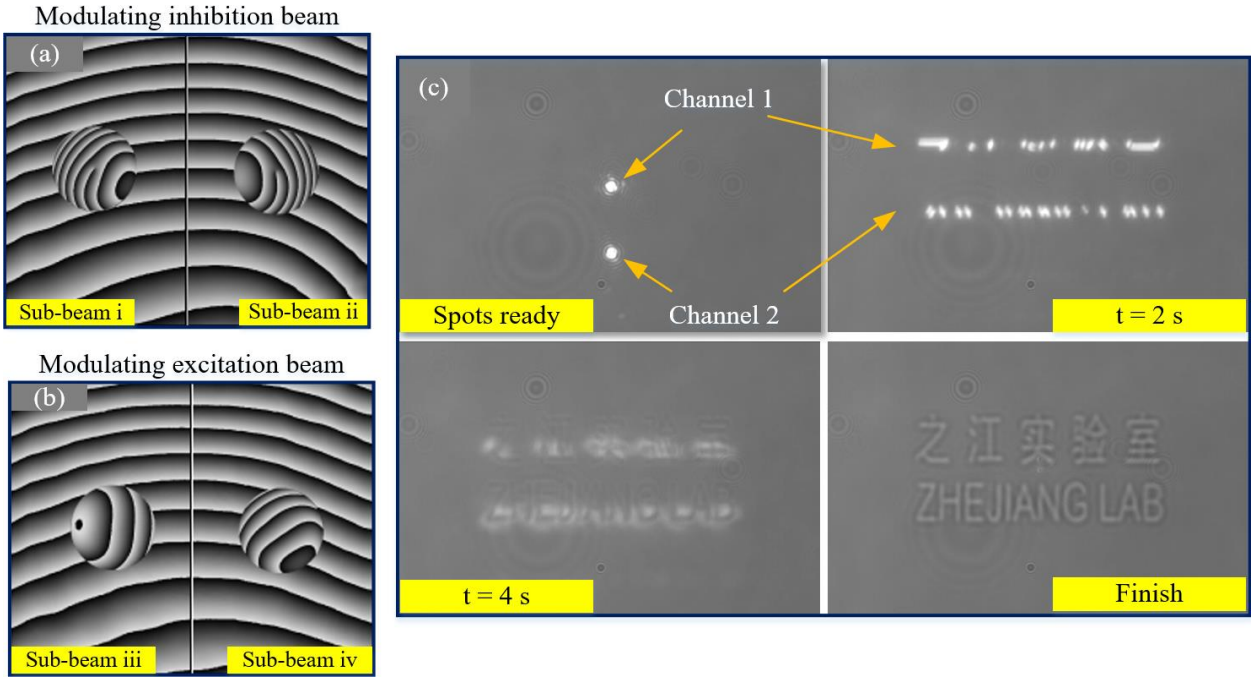

**Fig. S7** Phase masks and parallel printing process for the two lines of text: (a) and (b) phase masks loaded on SLMs; (c) snapshots of four instants during the printing process.

## 3 Three-Dimensional Dark Spot

Our system also supports traditional single-path three-dimensional (3D) enhancement using a 3D dark spot. When utilizing a 0–π annular phase mask to modulate the two 532-nm sub-beams, two dark spots for z-direction inhibition can be generated (Figs. S8(a) and S8(b)), corresponding to sub-beams i and ii, respectively. If the phase mask of sub-beam i is changed to a vortex and the two spots are superimposed, a 3D dark spot can be generated. Figures S8(c) and S8(d) show the combination of spots with different and same pseudo-colors, respectively. Figure S8(e) depicts the solid excitation spot.

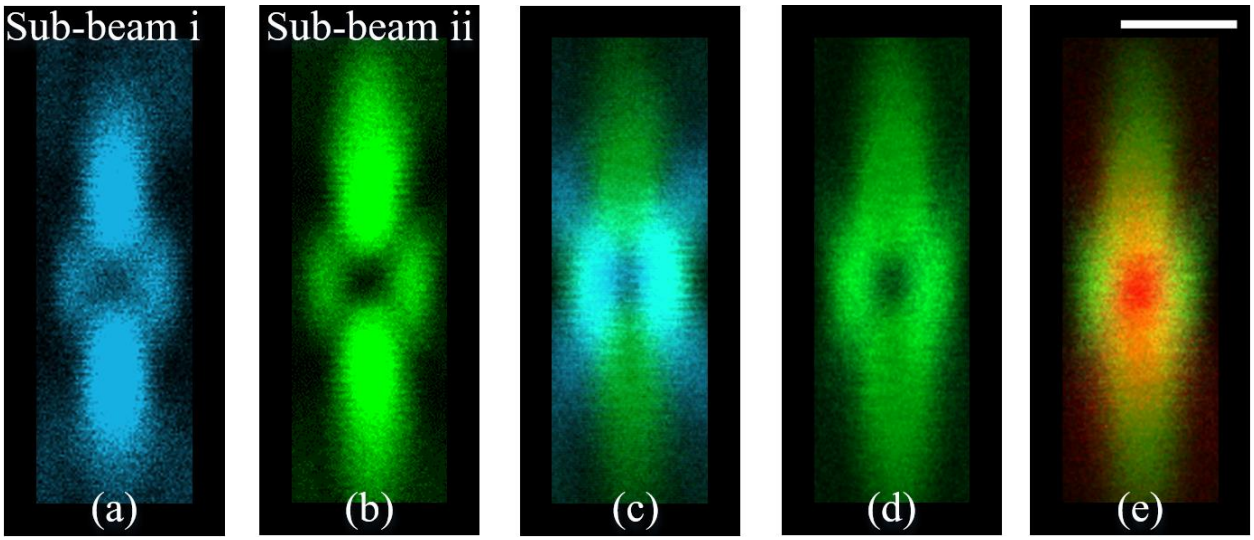


**Fig. S8** Three-dimensional dark spot x-z plane: (a) and (b) dark spot used for z-direction inhibition; (c) and (d) 3D dark spot formed by a combination of two spots with different and same pseudo-colors; (e) 3D dark spot with a solid excitation spot. Scale bar shared by all panels: 500 nm.

## 4 Suspended Nanowires in the Ladder Structure

To demonstrate the stability of our method and that it can achieve sub-50-nm feature size, we printed two ladder structures with and without peripheral photoinhibition (PPI); Figs. S9(a) and 3(b) present the respective SEM images. The corresponding enlarged views (Figs. S9(c) and S9(d)) indicate that the nanowires are reproducible, with line widths of ~35 and 60 nm. The powers of the excitation and inhibition spots were 2.69 and 0.83 mW, respectively, and the scanning speed was 1 mm/s.

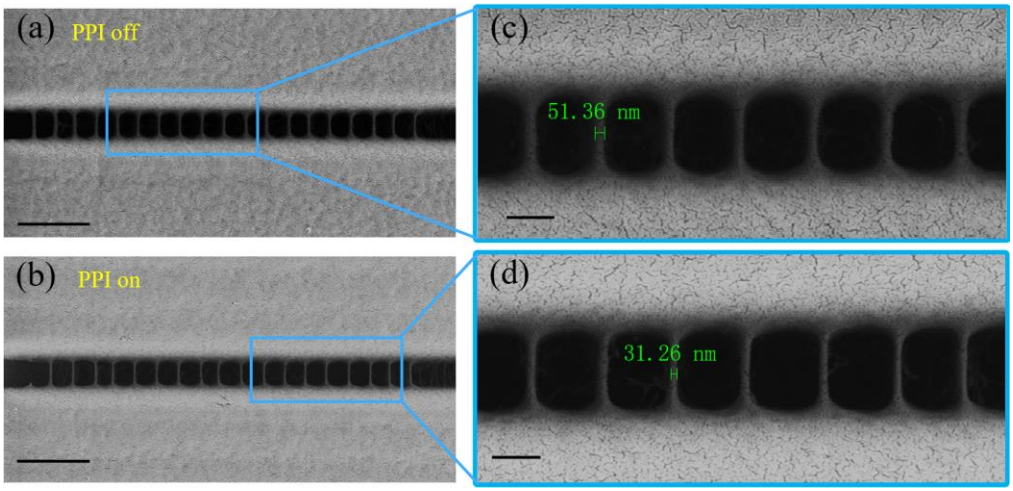


**Fig. S9** Results of printing suspended nanowires: (a) overall view without PPI; (b) overall view with PPI; (c) and (d) enlarged views of (a) and (b), respectively. Scale bar in (a) and (b), 1 μm; scale bar in (c) and (d), 200 nm.

## 5 Free-Standing Nanowires

Feature sizes <30 nm can also be obtained by our proposed $P^3L$ system, as indicated by the free-standing suspended nanowires shown in Fig. S10. Figure S10(a) demonstrates that the suspended line width can be compressed to <20 nm via PPI; however, this compression makes the structure very unstable. Figure S10(b) shows another free-standing nanowire with a more uniform line width (~25 nm) that is more stable. For the two free-standing suspended nanowires in Fig. S10, the

powers of the excitation and inhibition spots were identical (3.31 and 10.23 mW, respectively), and the scanning speed was 5 mm/s. For a given excitation wavelength, the final feature size is related to the photoresist properties, in addition to the power of the excitation and inhibition spots and the scanning speed. As the feature size decreases, the influence of the photoresist properties increases. It is worth noting that our system can provide a 68.9-nm 3D feature size with only 2PP-DLW.

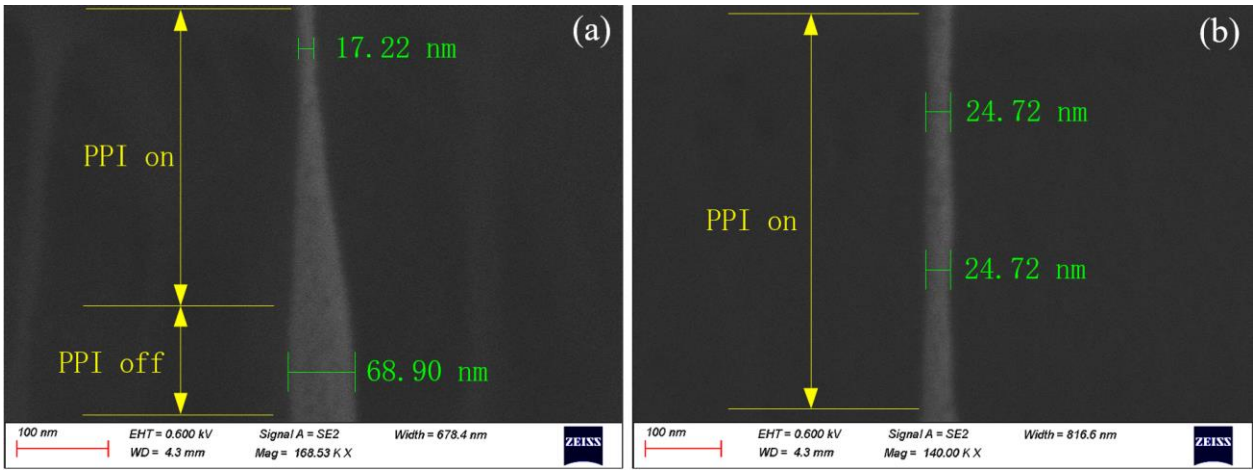


**Fig. S10** SEM images of free-standing suspended nanowires printed by the P$^3$L system. (a) Free-standing wire with a sub-20-nm line width. The first half of the nanowire was not printed with PPI; the other half was. After the PPI was turned on, the line width was compressed from 68.9 to 17.22 nm. (b) Free-standing wire with a sub-30-nm line width printed with PPI throughout.

## 6 Bit-Pattern Parallel Printing

In the results presented in Fig. 3 in the main text, the upper bit pattern was printed with PPI, whereas the lower line was not. Here, Fig. S11(a) presents SEM images of two additional bit dot patterns printed by two channels with PPI. The dwell time of one dot was 8 μs, the excitation spot power was 14.5 mW, and the inhibition power was 41.0 mW. A pattern consisting of two square waves with many bit dots separated by a distance of only 150 nm was also printed, as shown in

Fig. S11(b) and (c). Even though the pitch is less than that depicted in Fig. 3 by 50 nm and several accidental artifacts are evident (such as that in the red box in Fig. S11(b)), the upper square-wave pattern is clearly resolved, with distinct gaps; by contrast, the lower one is blurred and does not reveal any details. The two square-wave patterns were printed simultaneously. Subsequently, we changed the phase of one of the square waves, which resulted in a non-identical pattern. Because each beam in our system could print independently, the two different square waves could still be printed simultaneously. The powers of the excitation and inhibition spots were 19.4 and 51.7 mW, respectively, and the printing dwell time of each bit was 8 μs.

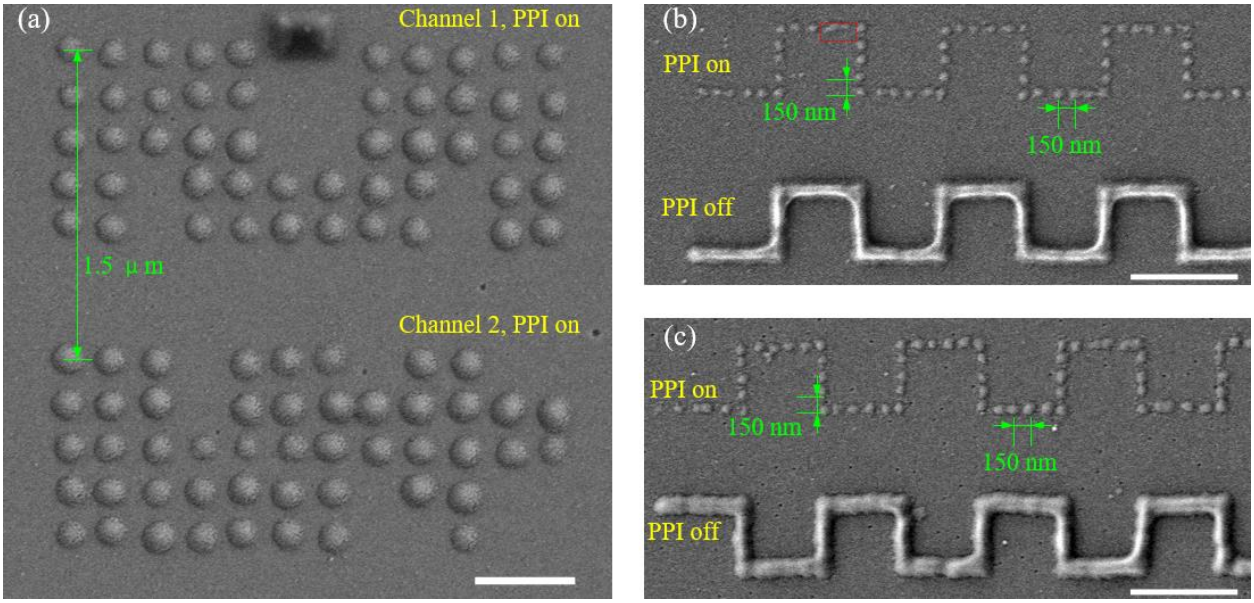


**Fig. S11** Bit-pattern printing results: (a) SEM images of two different patterns printed by two channels with PPI. Scale bar: 500 nm. (b) SEM image of the same pattern printed with and without PPI; (c) SEM image of two different patterns printed with and without PPI. In both, the top pattern was printed by channel 1 with PPI, whereas the bottom pattern was printed by channel 2 without PPI. The horizontal and vertical bit pitches are 200 nm in (a) and 150 nm in (b) and (c). Scale bars in (b) and (c) represent 1 μm. Red box in (b) indicates an artifact.

## 7 Printing Metamaterial Cubic Units

In addition to the cells shown in Fig. 4, a cell with 3 × 3 × 3 units was printed at a faster scanning speed of 150 mm/s (step size: 200 nm (x) × 200 nm (y) × 200 nm (z)), as shown in Fig. S12 (red box).

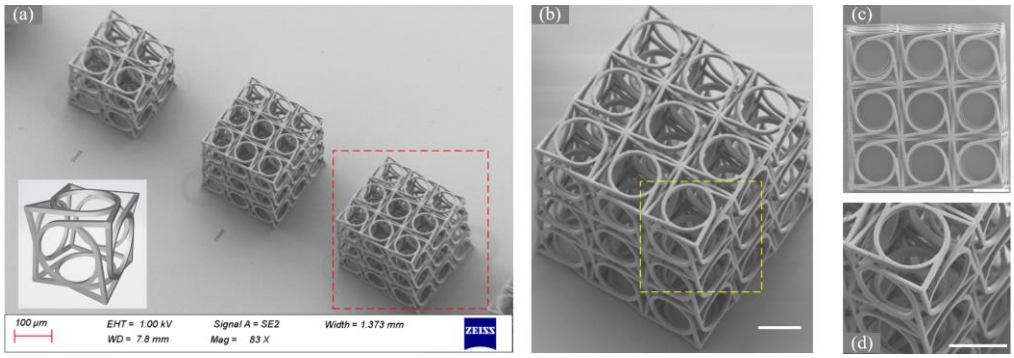


**Fig. S12** Metamaterial cubic printing results. (a) Raw SEM image of all cells. The inset shows the 3D model of a unit. (b) Enlarged view of the cell in the red box in (a), with a scanning speed 150 mm/s. (c) Top view of (b). (f) Zoomed-in view of the yellow box in (b). Scale bars: 50 µm.

## 8 Printing 2.5D Structures

We tested the feasibility of the system by printing some larger-scale structures with 2PP alone. Although these structures are normally referred to as 3D structures, we refer to them as 2.5D structures because they are similar to reliefs. Here, the separation distance of the two spots could be controlled using the phase map. However, the control distance was limited. We set it to 20 µm when using the 100× objective lens. At larger distances, the diffraction efficiency of the SLM would decrease significantly, which is not ideal. Figures S13(a) and S13(b) show two round structures: a propeller and a 40-µm-diameter Fresnel lens. The areas printed using different spots, indicated by different colors in Fig. S13(a), are the same in both cases. The single-spot power was 15 mW, and the speed was 10 mm/s (step size: 100 nm (x) × 100 nm (y) × 200 nm (z)). Next, a

lens array containing 12 × 12 lenses, as shown in Fig. S13(c), was printed using the same parameters, where the diameter of a single lens was 18 μm. In this array, 4 × 4 lenses were printed in one field of view (FOV) using two spots, and eight-fold FOV stitching was implemented using the x-y stage. Finally, another lens array containing 4 × 4 lenses with a larger scale was printed based on a 40× objective lens (Fig. S13(d)). The distance between the two spots was 50 μm, and the diameter of a single lens was 47 μm. The power of a single spot was 30.4 mW, and the scanning speed was 50 mm/s (step size: 100 nm (x) × 100 nm (y) × 200 nm (z)).

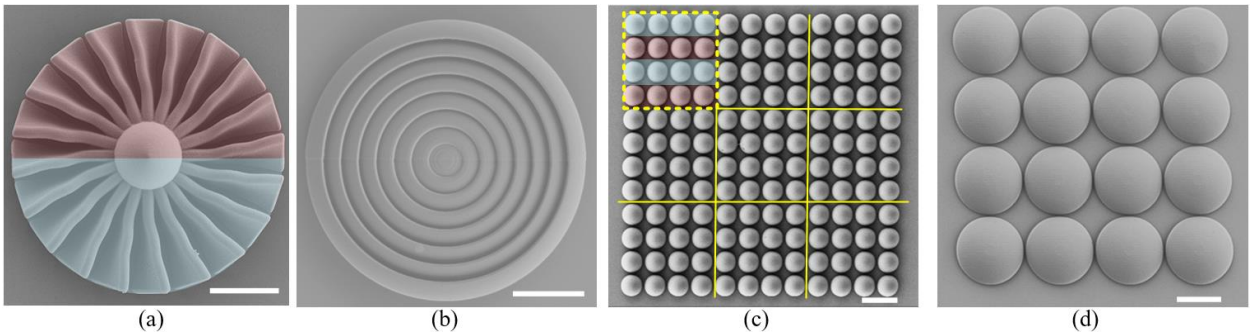


**Fig. S13** SEM image of 2.5D structures: (a) propeller; (b) Fresnel lens; (c) lens array; and (d) lens array printed by a 40× objective lens. Scale bar in (a) and (b): 10 μm; scale bar in (c) and (d): 30 μm. In (a), different colors show areas printed using different spots.